university of groningen

University Medical Center Groningen

University of Groningen

Scalable fabrication of high-quality crystalline and stable FAPbI(3) thin films by combining doctor-blade coating and the cation exchange reaction

Adjokatse, Sampson; Fang, Hong-Hua; Duim, Herman; Loi, Maria Antonietta

Published in:
Nanoscale

DOI:
10.1039/c8nr10267h

IMPORTANT NOTE: You are advised to consult the publisher's version (publisher's PDF) if you wish to cite from it. Please check the document version below.

Document Version
Final author's version (accepted by publisher, after peer review)

Publication date:
2019

Link to publication in University of Groningen/UMCG research database

Citation for published version (APA):
Adjokatse, S., Fang, H-H., Duim, H., & Loi, M. A. (2019). Scalable fabrication of high-quality crystalline and stable FAPbI(3) thin films by combining doctor-blade coating and the cation exchange reaction. *Nanoscale*, *11*(13), 5989-5997. https://doi.org/10.1039/c8nr10267h

Copyright
Other than for strictly personal use, it is not permitted to download or to forward/distribute the text or part of it without the consent of the author(s) and/or copyright holder(s), unless the work is under an open content license (like Creative Commons).

The publication may also be distributed here under the terms of Article 25fa of the Dutch Copyright Act, indicated by the “Taverne” license. More information can be found on the University of Groningen website: https://www.rug.nl/library/open-access/self-archiving-pure/taverne-amendment.

Take-down policy
If you believe that this document breaches copyright please contact us providing details, and we will remove access to the work immediately and investigate your claim.

Downloaded from the University of Groningen/UMCG research database (Pure): http://www.rug.nl/research/portal. For technical reasons the number of authors shown on this cover page is limited to 10 maximum.

Scalable fabrication of high-quality crystalline and stable $FAPbI_3$ thin films by combining doctor-blade coating and cation exchange reaction

Sampson Adjokatse, Hong-Hua Fang, Herman Duim, and Maria Antonietta Loi

Zernike Institute for Advanced Materials, University of Groningen, Nijenborgh 4, 9747 AG, Groningen, The Netherlands

Corresponding author: m.a.loi@rug.nl

Abstract

Formamidinium lead iodide ($FAPbI_3$) is one of the most extensively studied perovskite materials due to its narrow band gap and high absorption coefficient, which makes it highly suitable for optoelectronic applications. Deposition from a solution containing both lead iodide (PbI_2) and formamidinium iodide (FAI) or by sequential deposition of PbI_2 and FAI usually leads to the formation of films with poor morphology and unstable crystal structure that readily crystallizes into two different polymorphs: the photoinactive yellow phase and the photoactive black phase. In this work, two-dimensional (2D) 2-phenylethylammonium lead iodide (PEA_2PbI_4) thin films are deposited by a scalable doctor-blade coating technique and used as a growth template for the fabrication of high-quality 3D $FAPbI_3$ perovskite thin films, which are obtained by organic cation exchange. We report the structural, morphological and optical properties of these converted 3D $FAPbI_3$ perovskite films and compare them to the directly deposited 3D $FAPbI_3$ films. The converted $FAPbI_3$ thin films are compact, smooth, highly oriented and exhibit better structural stability in comparison to the directly deposited 3D films. These results do not only underscore the importance of the employed deposition techniques in the formation of highly crystalline and stable perovskite thin films but also reveal a strategy to easily obtain very compact perovskite layers using doctor-blade coating.

1. INTRODUCTION

Organic-inorganic metal halide perovskite semiconductors are of very high interest to the semiconductor community due to their superior photophysical properties and their ever-increasing significance for optoelectronic and other electronic applications.[1–4] Thin films of metal halide perovskites have been used extensively as light absorbers in photovoltaics[5–8] with certified record power conversion efficiency (PCE) of 23.7%.[9] Other optoelectronic devices in which perovskite semiconductors have been investigated and have demonstrated outstanding performances include light-emitting diodes,[10–12] light emitting field-effect transistors,[13–16] lasers,[17–20] photodetectors[21–25] and x-ray detectors.[26,27]

One of the key factors that has been central to the demonstrated device performances is the perovskite film quality. This includes the morphology, crystallinity and phase purity. In the last years, the most used deposition method has been the one-step solution processing technique, which involves direct deposition of the solution containing the perovskite precursors, typically lead halide (PbX_2, X = I^-, Br^-, Cl^-) and methylammonium halide (MAX) or formamidinium halide (FAX).[3,5] This technique results in the formation of thin films with poor surface coverage, large surface roughness and often unreacted PbX_2 residues, with negative consequences for performance and stability of devices.[28] To enhance the perovskite film quality, deposition techniques such as two-step sequential deposition, vapor-assisted deposition, and thermal vapor deposition techniques have been developed.[29–33] Other techniques such as solvent engineering[34–36], solvent additives[37] or temperature-assisted rapid nucleation[38] and process engineering methods like the anti-solvent treatment,[39] solvent annealing[40] and hot-casting[41] have all been advanced in order to control the film morphology and its quality in general.

An important problem is that the quality of films deposited by these techniques is dependent highly on the material composition and the solvent used, which is one of the main reasons for the large proliferation of deposition techniques. For instance, while high-quality perovskite films of methylammonium lead iodide ($MAPbI_3$) have been formed using most of the above-mentioned advanced processing techniques, only the sequential deposition method has given satisfactory formamidinium lead iodide ($FAPbI_3$) thin films.[42–46]

$FAPbI_3$ is a highly interesting material because of its band gap (~1.48 eV) and its enhanced thermal stability compared to the widely used $MAPbI_3$. However, the ionic radius and symmetry of the FA^+ cation makes $FAPbI_3$ perovskite structurally unstable as it can readily crystallize into two different polymorphs at room temperature: the undesired photoinactive “yellow” δ-phase (δ-$FAPbI_3$) and the desired photoactive “black” α-phase (α-$FAPbI_3$).[46,47] Thus, new strategies are required to fabricate and upscale high-quality $FAPbI_3$ thin films with improved morphology and structural stability, which could lead to enhanced optoelectronic properties, both in terms of performances and stability.

Recently, an avalanche of new processing techniques has been employed to control and grow high-quality perovskite thin films and also to tune their composition. One of such techniques is the incorporation of dopants such as Cs to structurally stabilize $FAPbI_3$ as demonstrated by Zhu and co-workers.[48] Alternative technique is the ion exchange reaction which is a well-known method for engineering material composition, creating alloys or obtain controlled doping.[49] $MAPbI_3$ thin films with high surface coverage, smoothness and crystallinity have been successfully fabricated using various starting materials as thin film growth templates.[50–53] Similarly, using $HPbI_3$, NH_4PbI_3,[54] $MAPbI_3$[55] etc., as growth

templates, various groups have demonstrated the fabrication of phase-pure α-$FAPbI_3$ thin films with enhanced film quality. Eperon *et al.*, have also successfully demonstrated the exchange of the B-site metal cation by partial or full substitution of tin (Sn) in formamidinium tin iodide ($FASnI_3$) with lead (Pb).[56] Jen and co-workers recently used 2D perovskite, namely, phenylethylammonium lead bromide (PEA_2PbBr_4) as growth template, demonstrating highly oriented, high-quality 3D methylammonium lead bromide ($MAPbBr_3$) thin films.[57]

At this point, it is important to underline, that all these techniques are based on a spin coating step and are difficult or impossible to scale up, which is a bottleneck towards the exploitation of hybrid perovskites in technology. Given the need for solution-based thin film deposition techniques that are simple, low-cost and compatible with industrial-scale fabrication, in this work we demonstrate an industrially relevant deposition pathway, giving rise to high quality hybrid perovskite thin films. This deposition pathway combines the advantages of doctor-blade coating and the ion exchange reaction method to fabricate high-quality phase-pure α-$FAPbI_3$ perovskite thin films that are structurally stable and highly crystalline. Phenylethylammonium lead iodide (PEA_2PbI_4) perovskite thin films are doctor-blade coated and fully converted to α-$FAPbI_3$ by immersing the 2D layer in a FAI solution. The choice of PEA_2PbI_4 as our starting material is based on its good film formability on different substrates even when deposited using different deposition techniques, including scalable blade coating. For comparison, one-step doctor-blade coated $FAPbI_3$ thin films are also investigated. The structural, morphological and optical characterization shows that the converted thin films exhibit unprecedented film quality, with preferential crystallographic orientation and enhanced ambient stability compared to the one-step deposited films. These results underline the immense potential of the combined blueprint of scalable doctor-blade coating and ion exchange reaction technique in the growth of stable and high-quality perovskite thin films.

2. EXPERIMENTAL

Materials and solution preparation

The perovskite precursors: lead (II) iodide (PbI_2) (99.99%), 2-phenylethylammonium iodide ($C_6H_5C_2H_4NH_3I$, PEAI) (>98%) and formamidine hydroiodide (FAI) (>98%) were purchased from TCI EUROPE N.V and were used as received without further purification. *N,N′*-Dimethylformamide (DMF) (99.8%) was acquired from Sigma-Aldrich and Dimethyl sulfoxide (DMSO) (99.9%) from Alfa Aesar.

The 2D PEA_2PbI_4 perovskite precursor solution was prepared by dissolving PEAI and PbI_2 at a molar ratio of 2:1 in a mixed solvent of DMF and DMSO at a volume ratio of 4:1 to form a solution of 0.5 M in concentration. The 3D $FAPbI_3$ perovskite precursor solution was prepared by dissolving FAI and PbI_2 at a molar ratio of 1:1 also in a mixed solvent of DMF and DMSO at a volume ratio of 4:1 to form a solution of 1 M in concentration. The solutions were stirred for at least 3 hours at room temperature before deposition. The organic precursor solution was prepared by dissolving FAI in isopropyl alcohol (IPA) to form a solution with a concentration of 20 mg mL^{-1}.

Perovskite film fabrication

The films were fabricated on glass substrates, which were ultrasonically cleaned in detergent solution, deionized water, acetone and isopropanol, sequentially. After drying them in an oven at 140 ^{o}C for about 10 min, they were treated with ultraviolet ozone (UV-O_3) for 20 min and then transferred into a nitrogen-filled glovebox immediately for the film deposition.

The perovskite growth process involved the transformation of pure 2D perovskite, PEA_2PbI_4 to the desired 3D $FAPbI_3$ perovskite thin film by ion exchange method. The 2D films were fabricated using spin coating and doctor blade coating techniques. The spin coated 2D samples were fabricated using a two-step spin program with anti-solvent treatment. The spin program was set at 1000 rpm for 10 s and 4000 rpm for 30 s. The anti-solvent (chlorobenzene) was dropped onto the film at about 10 s prior to the end of the spinning. The films were immediately annealed at 100 ^{o}C for 10 min. For the doctor blade coating process, the precursor solution was dropped onto the substrate and swiped linearly by a metal blade as depicted in Fig. 1. The optimized 2D films were blade coated onto glass substrates held at 80˚C by swiping the precursor solution with the blade at a speed of 10 mm s^{-1}. The gap between the glass substrate and the blade was fixed at 400 µm. The films were immediately annealed at 100 ^{o}C for 10 min. The optimized reference 3D $FAPbI_3$ perovskite film was also blade coated at a temperature of 90˚C with a blade speed of 40 mm s^{-1} and a fixed gap of 400 µm. The film was annealed at 160˚C for at least 30 min. To convert the 2D perovskite to 3D, the 2D film was dipped into 20 mg mL^{-1} FAI in IPA solution for ~ 3 min and then rinsed in IPA for ~ 30s in order to wash away dangling PEA^+ ions on the surface of the film and subsequently dried by spinning. No further annealing was required to drive the 3D conversion to full completion.

Morphological Characterization

The scanning electron microscopy (SEM) images were obtained using the FEI Nova Nano SEM 650 with an accelerating voltage of 2~10 kV for the secondary electron images and ~10 kV for the backscattered electron images. The Atomic force microscopy (AFM) images were taken using the Bruker NanoScope V in the ScanAsyst mode. Reflected light micrographs were recorded using an Olympus BX51M microscope equipped with a ColorView CCD camera and plan fluor objectives with 5x, 10x and 50x magnifications.

Structural Characterization

The X-ray diffraction experiment was performed in ambient conditions using a Bruker D8 Advanced diffractometer in Bragg-Brentano geometry and operating with Cu Kα radiation source (λ = 1.54 Å) and Lynxeye detector.

Optical Characterization

Absorption measurements were taken using UV-vis-NIR spectrophotometer (Shimadzu UV-3600). The photoluminescence measurements were performed using the second harmonic (400 nm) of a Ti:sapphire laser (repetition rate, 76 MHz; Mira 900, Coherent) to excite the samples. The illumination power could be adjusted using a variable neutral density filter. The excitation beam was spatially limited by an iris and focused with a 150-mm focal length

lens. Emitted photons were collected with a lens and directed to a spectrograph. Steady-state spectra were collected using a Hamamatsu EM-CCD camera.

Confocal laser scanning microscopy (CLSM) measurements were performed using a Nikon Eclipse Ti microscope. Samples were excited using an Ar+ laser with an excitation wavelength of 488 nm. The excitation beam was focused on the sample using a 100x (oil immersion Plan Apo) objective. Spatial mapping of the photoluminescence was obtained by raster scanning the sample and recording the PL signal using a 650 nm long pass detection channel.

3. RESULTS AND DISCUSSION

2D PEA_2PbI_4 perovskite thin films are fabricated from a solution containing 2-phenylethylammonium iodide (PEAI) and PbI_2 in a solvent mixture of *N*,*N*′-Dimethylformamide (DMF) and dimethyl sulfoxide (DMSO) using both spin coating and doctor-blade coating techniques. Unlike the 3D perovskites, this 2D material exhibited good film formability even when deposited using one-step solution deposition techniques. Fig. 1 shows the schematic diagram of the deposition procedure for the doctor-blade coating technique. The detailed fabrication procedure of the 2D films using both spin-coating and doctor-blade coating methods are described in the experimental section.

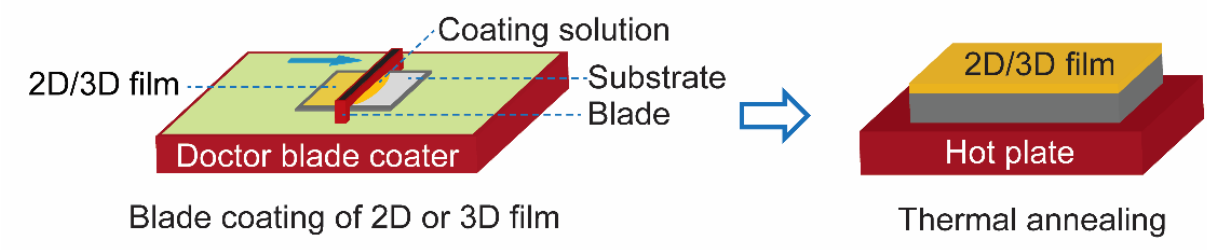

Fig. 1: Schematic illustration of the doctor-blade setup used for the deposition of the 2D PEA_2PbI_4 and reference 3D $FAPbI_3$ perovskite film.

The structure, morphology and band-gap of the prepared thin films are examined using x-ray diffraction (XRD), atomic force microscopy (AFM) and UV-Vis spectroscopy, respectively. The two deposition techniques result in thin films with similar XRD patterns and absorption profiles but very different morphology. As it is shown in Fig. S1(a), the XRD patterns of the two samples exhibit similar diffraction peaks with preferential orientation at 2θ values of 5.45˚, 10.88˚, 16.30˚, 21.79˚, 27.29˚, 32.92˚ and 38.56˚. However, the doctor-blade coated film exhibits more than three orders of magnitude stronger peak intensity compared to the spin coated film. This proves the higher crystallinity of the doctor-blade coated film.

The absorption spectra of these thin films closely resemble those previously reported with an excitonic peak at 515 nm.[58] The doctor-blade coated film however, has a higher

absorbance than the spin-coated film, implying that the film is thicker and/or has better surface coverage [Fig. S1(b)].

The morphological properties of the films are characterized using atomic force microscopy (AFM). While the spin coated film shows high inhomogeneity and roughness with surface grains of nanometer-sizes, the doctor-blade coated film is flatter, smoother and have crystalline domains that are as large as 15 µm as evident from Fig. S1(c) and S1(d)**,** respectively. The surface roughness of these films extracted from the AFM images are 22 and 50 nm in favor of the doctor-blade coated film.

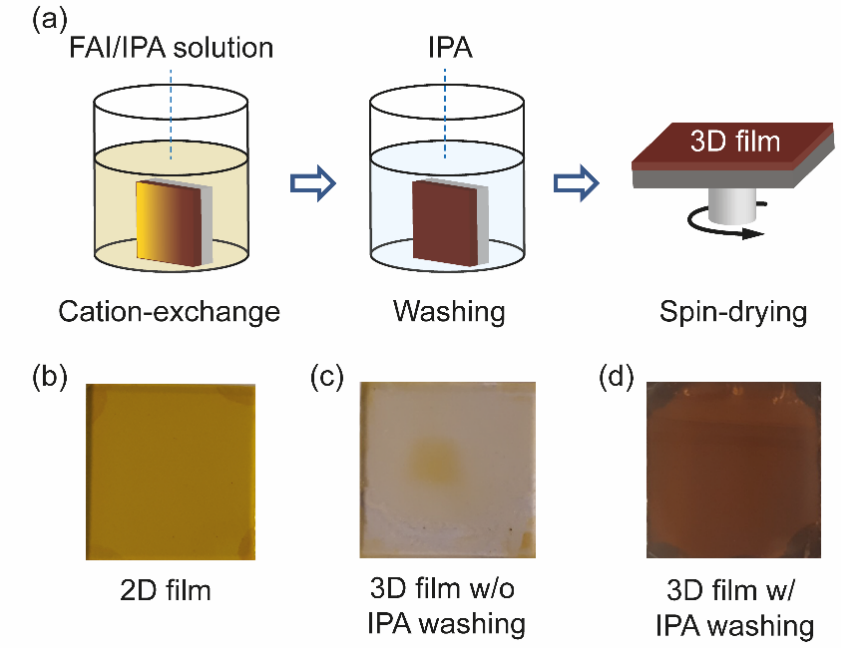

Fig. 2: **(a)** Schematic illustration of 2D to 3D conversion by cation exchange reaction. **(b)** Photographs of spin-dried 2D perovskite film, **(c)** converted 3D perovskite film without washing in isopropyl alcohol (IPA) and **(d)** converted 3D perovskite film with washing in IPA.

The 2D perovskite films are dipped into a solution containing FAI dissolved in isopropyl alcohol (IPA) to convert them into 3D $FAPbI_3$ perovskite by ion (organic-cation) exchange reaction. The approach follows previous works, where various 2D perovskites were used as starting materials to grow multidimensional (2D/3D)[59] or 3D[52,53,57] hybrid perovskites. The schematic of the ion exchange reaction process is depicted in Fig. 2(a). The photographs of the 2D perovskite films before and after conversion to 3D films without and with rinsing in IPA are shown in Fig. 2(b-d). We observed that without the washing steps in IPA, the 3D perovskite film degrades immediately after drying [Fig. 2(c)], while the washed samples remain stable for many days. This observation shows that the exchange reaction is kinetically driven and in the absence of the washing step, it will be thermodynamically driven backward to the starting material. We therefore attribute this unstable behaviour of the unwashed samples to the presence of long organic ligands on the surface of the film that

readily promotes further reactions that are detrimental to the stability of the converted 3D perovskite film.

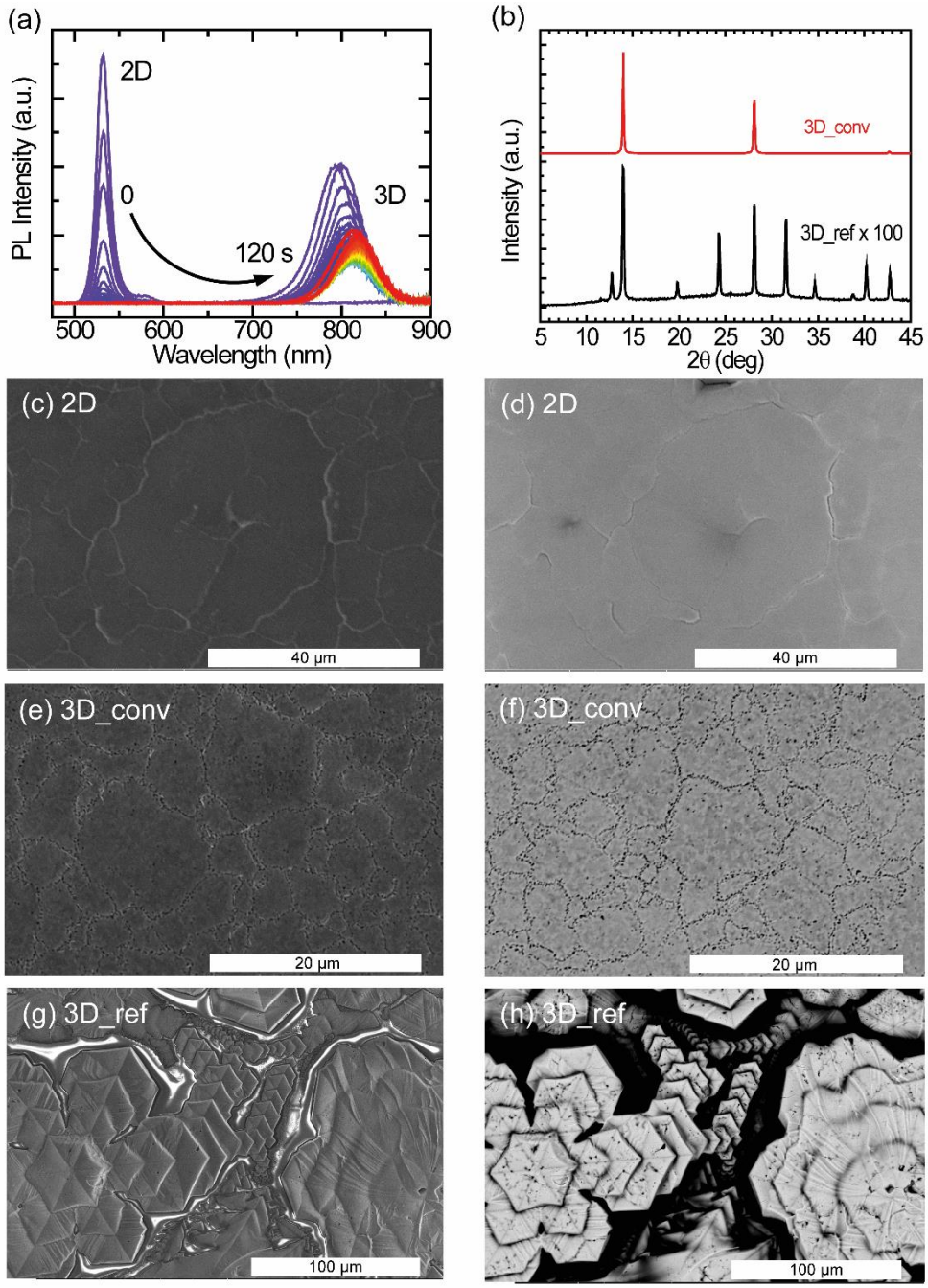

Fig. 3: 2D-3D conversion kinetics, structural and morphological characterization of converted and reference 3D perovskite films all fabricated with the doctor-blade coating technique. **(a)** In-situ photoluminescence (PL) emission spectra showing the conversion kinetics of the evolution from 2D to 3D perovskite, **(b)** X-ray diffraction pattern of the converted and of the reference film fabricated by doctor-blade coating. (**c-h**) SEM images showing the surface topography and compositional properties of the 2D PEA_2PbI_4, the converted and the reference 3D $FAPbI_3$ perovskite films. **(c, e** and **g)** Secondary electron and **(d, f** and **h)** backscattered electron images of the 2D, converted and reference 3D perovskite films, respectively.

To study the kinetics of the cation exchange in more detail, we performed an in-situ conversion experiment. At time $t = 0$, the FAI/IPA ligand solution is injected into a cuvette containing the 2D perovskite film to initiate the 2D to 3D conversion while simultaneously monitoring the photoluminescence (PL) of the sample. Fig. 3(a) shows the PL emission evolution of the conversion taken with 1-second time interval. Initially, only the narrow peak of the 2D perovskite at 530 nm is observed. The PL intensity of this 2D peak increases in the first second after adding the ligand solution but then vanishes almost completely within another 10 seconds. At the same time, a much broader PL peak originating from the 3D $FAPbI_3$ emerges around 800 nm. The emission from the 3D perovskite shows a rapid decrease in PL intensity and a considerable redshift in the first seconds after its appearance. A detailed analysis of the dynamics of the 3D peak can be found in the ESI [Fig. S2(a) and 2(b)]. After the appearance of the feature at around 800 nm, a minimum PL intensity is reached after 40 seconds as shown in Fig. S2(a). After this local minimum, the intensity steadily increases again while the peak continues exhibiting a small monotonic redshift [Fig. S2(b)]. This redshift is most likely caused by the conversion of low-dimensional perovskite intermediates to the 3D perovskite phase. It is important to underline that an eventual PL signal from the 2D and other low-dimensional perovskite phases, after the beginning of the conversion towards the 3D perovskite will not be directly detectable because of reabsorption and energy transfer. The slow recovery of PL in the final stage of the conversion process is considered to be the result of further growth of the 3D domains and minimization of defects through laser-induced healing.

After the full conversion from the 2D to 3D, the films are characterized to investigate the quality of the films. The comparison of the converted 3D films based on the spin coated and doctor-blade coated 2D films show that the later exhibit better film properties, mimicking the quality of the 2D films. The structural and morphological characteristics of the converted film based on the spin coated 2D film are shown in Fig. S3 of the ESI. As a reference for the converted films based on the doctor-blade coated 2D films, 3D $FAPbI_3$ thin films were doctor-blade coated on a glass substrate.

The XRD patterns illustrating the structural properties of the converted and reference 3D perovskite films fabricated by doctor-blade coating are displayed in Fig. 3(b). Compared to the reference film, the converted film exhibit highly oriented crystal domains with characteristic peaks at 2θ values of 13.97°, 28.13° and 42.71°, corresponding to scattering from (111), (222) and (333) crystal planes. The reference film, on the other hand, exhibits additional diffraction peaks at 12.74°, 19.79°, 24.30°, 31.56°, 34.65°, 38.81° and 40.22°, which correspond to randomly arranged crystal planes. Although no signature peak of the photoinactive (δ-phase) perovskite is observed in both films, the characteristic peak from PbI_2 (12.74°), which is a result of the rapid degradation of the sample in air, is observed for the reference film. The diffraction peaks from the converted films are about two orders of magnitude stronger in intensity than the one of the reference film. In Fig. 3(b), the peak intensity of the reference film is magnified by a factor of 100 for the purpose of illustration. The FWHM of the characteristic peak at 13.97° is 0.14° and 0.21° for the converted and the reference sample, respectively. This shows that the converted perovskite film has better crystallinity, and lower level of disorder with respect to the reference sample. It's worth mentioning at this point, that no diffraction peaks from the 2D perovskite are observed in the diffraction pattern of the converted film.

As explained above, the morphological quality of thin films defines the success of a deposition technique. The SEM images portraying the film topography (secondary electrons) and the composition (backscattered electrons) of the 2D, converted 3D and the reference 3D perovskite films are shown in Fig. 3**.** In Fig. 3(c), the secondary electron image of the 2D perovskite depicts a continuously smooth and homogeneous film with excellent surface coverage and very large crystalline domains (> 10 µm), consistent with that seen in the AFM images. The uniform brightness of the backscattered electron images also reflects the highly uniform compositional distribution of the 2D film [Fig. 3(d)]. These morphological features are directly translated to the converted 3D films except for the domain sizes, which appear smaller (> 3 µm) and the presence of pinhole-like features at the domain boundaries as shown in Fig. 3(e) and 3(f) for the secondary electron and backscattered electron images, respectively. SEM images showing a wider view of the converted film are shown in Fig. S4. The roughness of the converted 3D film as extracted from the AFM topographical image (Fig. S5) is approximately 40 nm. Interestingly, laser scanning confocal microscopy measurements performed on the converted film shows that the pitted domain boundaries have brighter photoluminescence (see Fig. S6**).** In stark contrast, the topographical image of the 3D reference film in Fig. 3(g) shows the formation of hexagonal-like crystalline domains, resulting in a non-uniform film. As revealed in the backscattered electron image of Fig. 3(h), the surface coverage of the film is very poor.

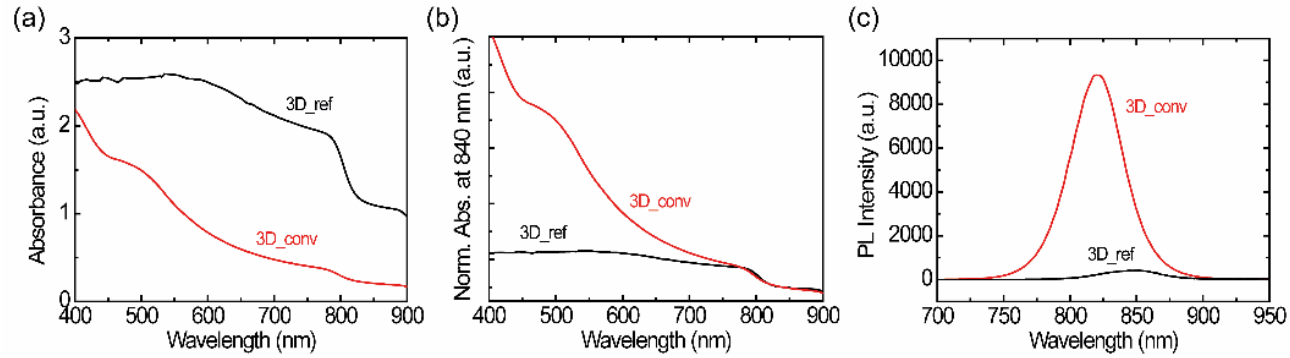

Fig. 4: Optical characterization of converted and reference 3D perovskite films on glass substrates. (**a**-**b**) UV-vis absorbance spectra without normalization (**a**) and with normalization at 840 nm (**b**), (**c**) Steady-state PL spectra. Note that 3D_ref and 3D_conv as indicated in figures denote the reference one-step coated and converted $FAPbI_3$ perovskite respectively.

The absorbance spectra of the converted and reference 3D $FAPbI_3$ perovskite films are shown in Fig. 4(a). The spectra are normalized at 840 nm to aid in the comparison of the spectral shape and estimation of the band-edge [see Fig. 4(b)]. The films have an absorption band-edge around 830 nm, confirming the formation of 3D $FAPbI_3$ perovskite. However, the spectral profiles of the films are very different. The converted film has a characteristic absorption profile that depicts a continuous increase in light absorption from the near-infrared (NIR) to the visible region while the reference film shows an almost constant light absorption in the same range. Moreover, as it is shown in Fig. 4(a), the reference film has a

very high background signal in the NIR compared to the converted film. These features are directly related to the film quality, specifically, the degree of surface coverage and homogeneity. While the observed high background absorption from the reference film is attributed to the high inhomogeneity of the film, which gives rise to large scattering of the incident light, the flattening of the spectrum is attributed to poor surface coverage. These observations are in agreement with previous studies by Tian *et al*., where the correlation between absorption spectral shapes and surface coverage and inhomogeneity of $MAPbI_3$ perovskite thin films are examined.[60]

Fig. 4(c) shows the photoluminescence spectra of both the reference and the converted film upon excitation with a 400 nm laser. The converted film shows a PL intensity that is over 20 times higher than that of the reference film. This large difference in PL intensity has two main causes; firstly, as mentioned before, the converted film shows much higher surface coverage than the reference film. Therefore, more photons are absorbed in the converted film and the PL intensity scales accordingly. Secondly, as the quality of the converted film is better than that of the reference film, it is to be expected that the excited charge carriers suffer less from non-radiative recombination in this film. This notion is further confirmed by the large redshift of the PL spectrum of the reference film (845 nm) with respect to that of the converted film (823 nm), such a redshift is typically associated with a high density of trap states.[57]

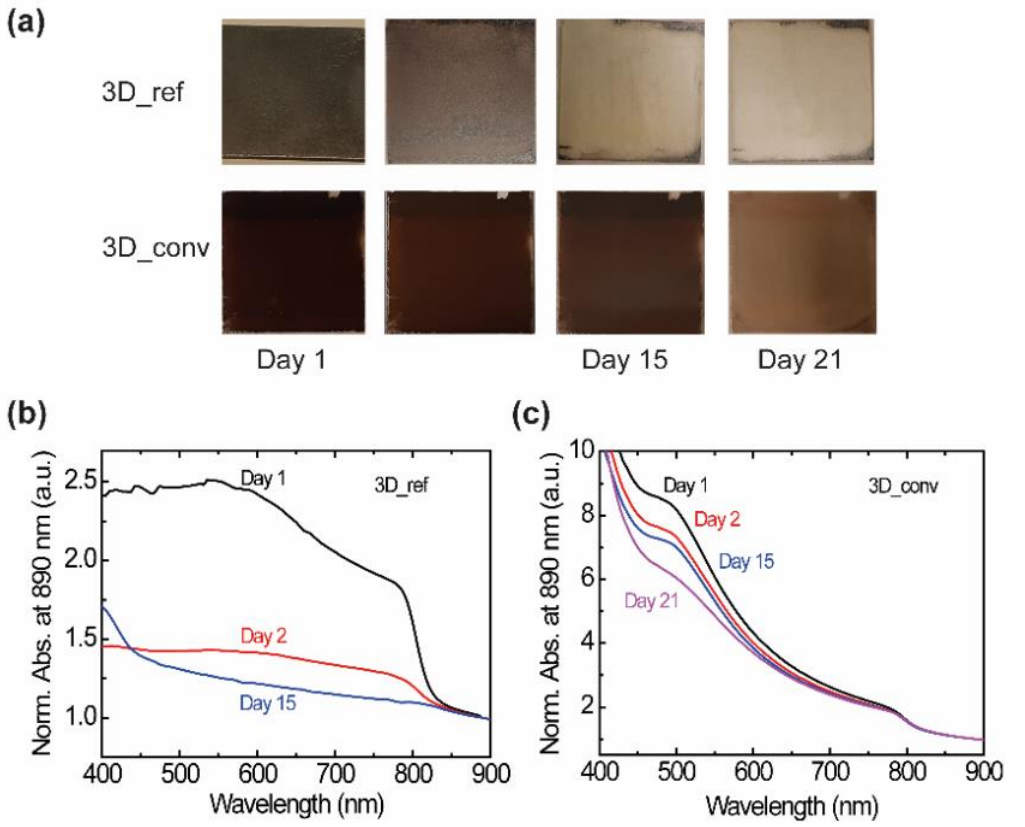

Fig. 5: Characterization of the moisture stability of the reference and converted 3D FAPbI3 perovskite films under ambient conditions. (**a**) Photographs showing the evolution of color of the reference (top) and converted (bottom) perovskite films over a 21-day period. (**b** and **c**) UV-vis absorbance spectra of the reference (**b)** and the converted (**c**) films normalized at 890 nm.

At this point it is interesting to verify if the stability of the material is also affected by the preparation method. The stability under ambient conditions is evaluated by probing the changes in the absorbance of the films under a relative humidity (RH) of 40~50% and temperature of ~23˚C. It is worth noting that the stability test under ambient conditions is performed on several films and a clear correlation of the film degradation over time on the quality of the film is found. Photographs of the most stable converted and reference films stored in air over a period of 21 days are presented in Fig. 5(a). Whereas the best of the reference film degraded rapidly within a day with consequent severe color bleaching, the best converted sample showed minimal degradation with negligible change in color even after 15 days. We attribute the degradation to the penetration of moisture at the grain or domain boundaries. The corresponding absorbance spectra of the films are shown in Fig. 5(b) and 5(c) for the reference and converted films, respectively. The absorbance of the reference film dropped drastically on the second day and as shown, no absorption peak was observed after 15 days. On the contrary, the converted film as already indicated by the photographs, maintained a high absorbance without spectral modification for 21 days as shown in Fig. 5(c).

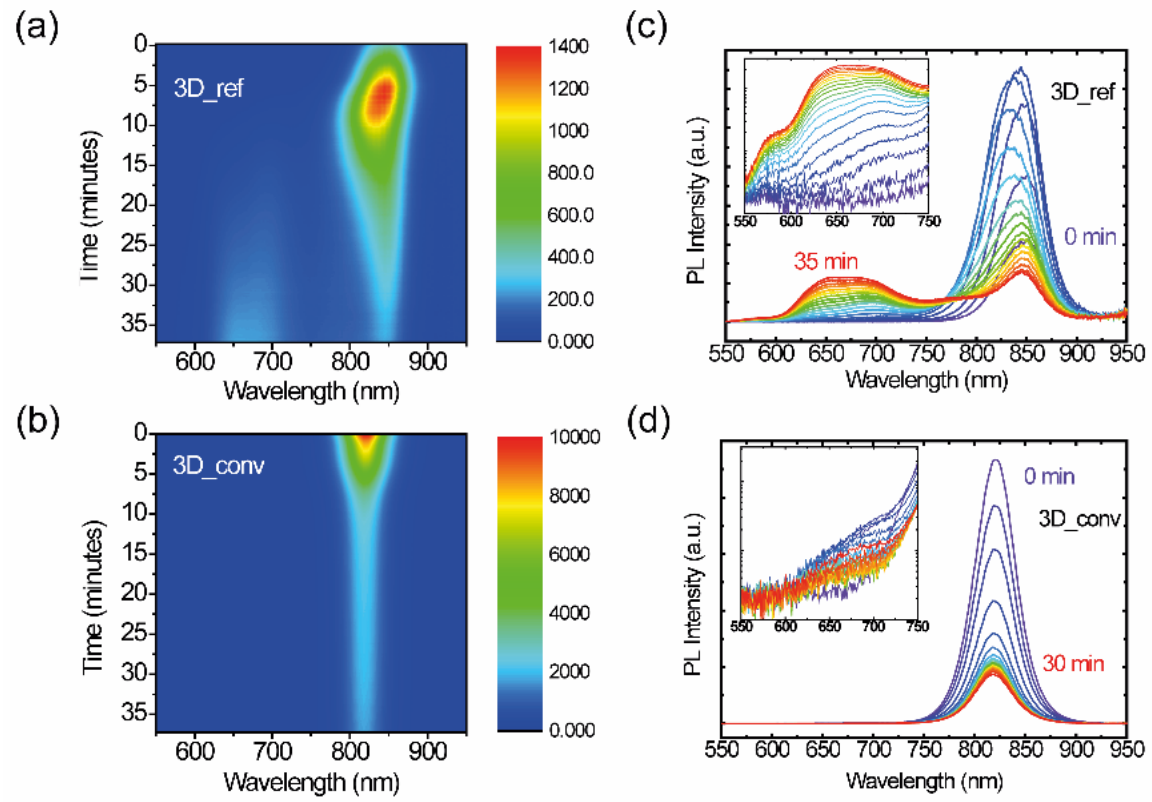

Fig. 6: Photostability of the reference and converted 3D FAPbI3 perovskite films. **(a)** 2D pseudo-color plot of the PL spectra of the reference film as a function of continuous laser excitation time. **(b)** 2D pseudo-color plot of the PL spectra of the converted film as a function of continuous laser excitation time. **(c)** Evolution of the PL spectra of the reference film. **(d)** Evolution of the PL spectra of the converted film.

Furthermore, the stability under illumination of both the converted 3D and reference films was assessed by exposing them to a focused laser beam of 400 nm (2.5 μJ cm^{-2}) wavelength, in ambient condition. Fig. 6 displays color maps of the PL spectra as a function of exposure time for (a) the 3D reference sample and (b) the converted film. PL spectra at selected time intervals are plotted alongside in (c) and (d). It is evident from these plots that the films behave distinctly different under illumination. In the case of the reference 3D film, the low PL initially increases due to the laser-induced healing of trap states, which is accompanied by a slight blue shift of the emission. After this initial healing stage, however, degradation begins and the intensity steadily drops until the signal reaches about 20% of its maximum intensity. During this degradation phase, a broad emission feature gradually arises at high energy, as is highlighted in the inset of Fig. 6(c). We assign this feature to degradation products of $FAPbI_3$, the most likely being PbI_2, resulting from evaporation of the volatile organic cation as observed in the case of $MAPbI_3$.[61,62] At the laser excitation point, the decomposition of the perovskite is visible by eye as a yellow spot. A cross-polarized light micrograph showing the strong change in birefringence of this degraded spot is shown in the ESI (Fig. S7). In stark contrast to this, the converted film only shows a steady decrease in PL intensity and no degradation byproduct can be observed under the same excitation conditions. Moreover, it should be noted that even after prolonged laser illumination, the final PL intensity of the converted film is still considerably higher than the maximal value that the reference film ever reaches, which again highlights the superior quality of the converted films. Furthermore, the substantially higher PL intensity, narrower FWHM and the blue-shifted emission wavelength as shown in Fig. S8 all indicate the superior quality of the converted film with respect to the reference film.

We can therefore conclude that the here reported conversion mechanism from a highly crystalline 2D film gives rise to highly oriented 3D films with superior ambient and photo-stability.

4. CONCLUSION

In summary, doctor-blade coated 2D 2-phenylethylammonium lead iodide (PEA_2PbI_4) films are employed as a growth template to fabricate high-quality photoactive 3D $FAPbI_3$ thin films using a cation exchange reaction. The resultant perovskite film exhibits better film formability, excellent surface coverage and improved morphology with crystalline domain sizes as large as ~10 μm. XRD patterns of the converted 3D perovskite film reveal very high crystallinity and highly preferential orientation that mimics the orientation of the 2D perovskite template. The improved perovskite film leads to enhanced photoluminescence intensity, about 20 times higher than the one of the reference one-step blade-coated $FAPbI_3$ perovskite film. Furthermore, stability studies under continuous laser illumination and under ambient conditions show that the converted film exhibits a significantly enhanced photo- and moisture stability compared to the reference film. The enhanced optoelectronic quality and high stability of the phase-pure $FAPbI_3$ perovskite thin films obtained by cation exchange reaction of a doctor-blade coated thin film is of extreme importance toward the engineering and stabilization of perovskite thin films for optoelectronic applications.

REFERENCES

[1] M. M. Lee, J. Teuscher, T. Miyasaka, T. N. Murakami, H. J. Snaith, *Science.* **2012**, *338*, 643.

[2] J. H. Noh, S. H. Im, J. H. Heo, T. N. Mandal, S. Il Seok, *Nano Lett.* **2013**, *13*, 1764.

[3] G. E. Eperon, S. D. Stranks, C. Menelaou, M. B. Johnston, L. M. Herz, H. J. Snaith, *Energy Environ. Sci.* **2014**, *7*, 982.

[4] G. Xing, N. Mathews, S. Sun, S. S. Lim, Y. M. Lam, M. Grätzel, S. Mhaisalkar, T. C. Sum, *Science* **2013**, *342*, 344.

[5] A. Kojima, K. Teshima, Y. Shirai, T. Miyasaka, *J. Am. Chem. Soc.* **2009**, *131*, 6050.

[6] B. G. H. M. Groeneveld, M. Najafi, B. Steensma, S. Adjokatse, H.-H. Fang, F. Jahani, L. Qiu, G. H. ten Brink, J. C. Hummelen, M. A. Loi, *APL Mater.* **2017**, *5*, 076103.

[7] S. Shao, M. Abdu-Aguye, T. S. Sherkar, H.-H. Fang, S. Adjokatse, G. ten Brink, B. J. Kooi, L. J. A. Koster, M. A. Loi, *Adv. Funct. Mater.* **2016**, *26*, 8094.

[8] S. Shao, Z. Chen, H.-H. Fang, G. H. Ten Brink, D. Bartesaghi, S. Adjokatse, L. J. A. Koster, B. J. Kooi, A. Facchetti, M. A. Loi, *J. Mater. Chem. A* **2015**, *4*, 2419.

[9] Research Cell Efficiency Records. National Renewable Energy Laboratory. https://www.nrel.gov/pv/assets/pdfs/pv-efficiency-chart.20181214.pdf, **2018**, (Accessed on 16 Dec 2018).

[10] G. Li, Z. Tan, D. Di, M. L. Lai, L. Jiang, J. H. Lim, R. H. Friend, N. C. Greenham, *Nano Lett.* **2015**, *15*, 2640.

[11] O. A. Jaramillo-Quintero, R. S. Sánchez, M. Rincón, I. Mora-Sero, *J. Phys. Chem. Lett.* **2015**, *6*, 1883.

[12] Z.-K. Tan, R. S. Moghaddam, M. L. Lai, P. Docampo, R. Higler, F. Deschler, M. Price, A. Sadhanala, L. M. Pazos, D. Credgington, F. Hanusch, T. Bein, H. J. Snaith, R. H. Friend, *Nat. Nanotechnol.* **2014**, *9*, 687.

[13] X. Y. Chin, D. Cortecchia, J. Yin, A. Bruno, C. Soci, *Nat. Commun.* **2015**, *6*, 7383.

[14] F. Li, C. Ma, H. Wang, W. Hu, W. Yu, A. D. Sheikh, T. Wu, *Nat. Commun.* **2015**, *6*, 8238.

[15] F. Maddalena, X. Y. Chin, D. Cortecchia, A. Bruno, C. Soci, *ACS Appl. Mater. Interfaces* **2018**, *10*, 37316.

[16] M. U. Chaudhry, K. Tetzner, Y.-H. Lin, S. Nam, C. Pearson, C. Groves, M. C. Petty, T. D. Anthopoulos, D. D. C. Bradley, *ACS Appl. Mater. Interfaces* **2018**, *10*, 18445.

[17] S. Chen, K. Roh, J. Lee, W. K. Chong, Y. Lu, N. Mathews, T. C. Sum, A. Nurmikko, *ACS Nano* **2016**, *10*, 3959.

[18] Y. J. Li, Y. Lv, C.-L. Zou, W. Zhang, J. Yao, Y. S. Zhao, *J. Am. Chem. Soc.* **2016**, *138*, 2122.

[19] H. Zhu, Y. Fu, F. Meng, X. Wu, Z. Gong, Q. Ding, M. V Gustafsson, M. T. Trinh, S. Jin, X.-Y. Zhu, *Nat. Mater.* **2015**, *14*, 636.

[20] P. Brenner, M. Stulz, D. Kapp, T. Abzieher, U. W. Paetzold, A. Quintilla, I. A. Howard, H. Kalt, U. Lemmer, *Appl. Phys. Lett.* **2016**, *109*, 141106.

[21] S. Yakunin, L. Protesescu, F. Krieg, M. I. Bodnarchuk, G. Nedelcu, M. Humer, G. De Luca, M. Fiebig, W. Heiss, M. V Kovalenko, *Nat. Commun.* **2015**, *6*, 8056.

[22] C. Li, C. Han, Y. Zhang, Z. Zang, M. Wang, X. Tang, J. Du, *Sol. Energy Mater. Sol. Cells* **2017**, *172*, 341.

[23] H. Lu, W. Tian, F. Cao, Y. Ma, B. Gu, L. Li, *Adv. Funct. Mater.* **2016**, *26*, 1296.

[24] H. Sun, T. Lei, W. Tian, F. Cao, J. Xiong, L. Li, *Small* **2017**, *13*, 1701042.

[25] Y. Fang, J. Huang, *Adv. Mater.* **2015**, *27*, 2804.

[26] S. Yakunin, M. Sytnyk, D. Kriegner, S. Shrestha, M. Richter, G. J. Matt, H. Azimi, C. J. Brabec, J. Stangl, M. V Kovalenko, W. Heiss, *Nat. Photonics* **2015**, *9*, 444.

[27] H. Wei, Y. Fang, P. Mulligan, W. Chuirazzi, H.-H. Fang, C. Wang, B. R. Ecker, Y. Gao, M. A. Loi, L. Cao, J. Huang, *Nat. Photonics* **2016**, *10*, 333.

[28] F. Liu, Q. Dong, M. K. Wong, A. B. Djurišić, A. Ng, Z. Ren, Q. Shen, C. Surya, W. K. Chan, J. Wang, A. M. C. Ng, C. Liao, H. Li, K. Shih, C. Wei, H. Su, J. Dai, *Adv. Energy Mater.* **2016**, *6*, 1502206.

[29] J. Burschka, N. Pellet, S.-J. Moon, R. Humphry-Baker, P. Gao, M. K. Nazeeruddin, M. Grätzel, *Nature* **2013**, *499*, 316.

[30] Z. Xiao, C. Bi, Y. Shao, Q. Dong, Q. Wang, Y. Yuan, C. Wang, Y. Gao, J. Huang, *Energy Environ. Sci.* **2014**, *7*, 2619.

[31] Q. Chen, H. Zhou, Z. Hong, S. Luo, H.-S. Duan, H.-H. Wang, Y. Liu, G. Li, Y. Yang, *J. Am. Chem. Soc.* **2014**, *136*, 622.

[32] M. Liu, M. B. Johnston, H. J. Snaith, *Nature* **2013**, *501*, 395.

[33] C.-W. Chen, H.-W. Kang, S.-Y. Hsiao, P.-F. Yang, K.-M. Chiang, H.-W. Lin, *Adv. Mater.* **2014**, *26*, 6647.

[34] N. J. Jeon, J. H. Noh, Y. C. Kim, W. S. Yang, S. Ryu, S. Il Seok, *Nat. Mater.* **2014**, *13*, 897.

[35] Y. Rong, Z. Tang, Y. Zhao, X. Zhong, S. Venkatesan, H. Graham, M. Patton, Y. Jing, A. M. Guloy, Y. Yao, *Nanoscale* **2015**, *7*, 10595.

[36] Y. Ren, B. Duan, Y. Xu, Y. Huang, Z. Li, L. Hu, T. Hayat, H. Wang, J. Zhu, S. Dai, *Sci. China Mater.* **2017**, *60*, 392.

[37] J. A. Love, S. D. Collins, I. Nagao, S. Mukherjee, H. Ade, G. C. Bazan, T. Q. Nguyen, *Adv Mater* **2014**, *26*, 7308.

[38] Y.-K. Ren, X.-H. Ding, Y.-H. Wu, J. Zhu, T. Hayat, A. Alsaedi, Y.-F. Xu, Z.-Q. Li, S.-F. Yang, S.-Y. Dai, *J. Mater. Chem. A* **2017**, *5*, 20327.

[39] D. Shi, V. Adinolfi, R. Comin, M. Yuan, E. Alarousu, A. Buin, Y. Chen, S. Hoogland, A. Rothenberger, K. Katsiev, Y. Losovyj, X. Zhang, P. A. Dowben, O. F. Mohammed, E. H. Sargent, O. M. Bakr, *Science* **2015**, *347*, 519.

[40] Z. Xiao, Q. Dong, C. Bi, Y. Shao, Y. Yuan, J. Huang, *Adv. Mater.* **2014**, *26*, 6503.

[41] W. Nie, H. Tsai, R. Asadpour, J.-C. Blancon, A. J. Neukirch, G. Gupta, J. J. Crochet, M.

Chhowalla, S. Tretiak, M. A. Alam, H.-L. Wang, A. D. Mohite, *Science* **2015**, *347*, 522.

[42] G. E. Eperon, C. E. Beck, H. J. Snaith, *Mater. Horizons* **2016**, *3*, 63.

[43] Y. Wu, A. Islam, X. Yang, C. Qin, J. Liu, K. Zhang, W. Peng, L. Han, *Energy Environ. Sci.* **2014**, *7*, 2934.

[44] M. Hu, L. Liu, A. Mei, Y. Yang, T. Liu, H. Han, *J. Mater. Chem. A* **2014**, *2*, 17115.

[45] L. Hu, J. Peng, W. Wang, Z. Xia, J. Yuan, J. Lu, X. Huang, W. Ma, H. Song, W. Chen, Y.-B. Cheng, J. Tang, *ACS Photonics* **2014**, *1*, 547.

[46] A. Binek, F. C. Hanusch, P. Docampo, T. Bein, *J. Phys. Chem. Lett.* **2015**, *6*, 1249.

[47] D. B. Mitzi, *Progress in Inorganic Chemistry. Volume 48*, John Wiley & Sons, Inc., **1999**.

[48] Z. Li, M. Yang, J.-S. Park, S.-H. Wei, J. J. Berry, K. Zhu, *Chem. Mater.* **2016**, *28*, 284.

[49] C. E. Harland, *Ion Exchange: Theory and Practice*, Royal Society Of Chemistry, Cambridge, **1994**.

[50] S. Pang, Y. Zhou, Z. Wang, M. Yang, A. R. Krause, Z. Zhou, K. Zhu, N. P. Padture, G. Cui, *J. Am. Chem. Soc.* **2016**, *138*, 750.

[51] Y. Zong, Y. Zhou, M. Ju, H. F. Garces, A. R. Krause, F. Ji, G. Cui, X. C. Zeng, N. P. Padture, S. Pang, *Angew. Chemie Int. Ed.* **2016**, *55*, 14723.

[52] F. Li, Y. Zhang, K.-J. Jiang, C. Zhang, J.-H. Huang, H. Wang, H. Fan, P. Wang, Y. Chen, W. Zhao, X. Li, L.-M. Yang, Y. Song, Y. Li, *Adv. Mater.* **2018**, *30*, 1804454.

[53] Y. Zhang, F. Li, K.-J. Jiang, J.-H. Huang, H. Wang, H. Fan, P. Wang, C.-M. Liu, L.-P. Zhang, Y. Song, *J. Mater. Chem. A* **2018**, *6*, 17867.

[54] Z. Zhou, S. Pang, F. Ji, B. Zhang, G. Cui, *Chem. Commun.* **2016**, *52*, 3828.

[55] Y. Zhou, M. Yang, S. Pang, K. Zhu, N. P. Padture, *J. Am. Chem. Soc.* **2016**, *138*, 5535.

[56] G. E. Eperon, D. S. Ginger, *ACS Energy Lett.* **2017**, *2*, 1190.

[57] T. Zhao, H. Liu, M. E. Ziffer, A. Rajagopal, L. Zuo, D. S. Ginger, X. Li, A. K. Y. Jen, *ACS Energy Lett.* **2018**, *3*, 1662.

[58] K. T. Cho, G. Grancini, Y. Lee, E. Oveisi, J. Ryu, O. Almora, M. Tschumi, P. A. Schouwink, G. Seo, S. Heo, J. Park, J. Jang, S. Paek, G. Garcia-Belmonte, M. K. Nazeeruddin, *Energy Environ. Sci.* **2018**, *11*, 952.

[59] T. M. Koh, V. Shanmugam, J. Schlipf, L. Oesinghaus, P. Müller-Buschbaum, N. Ramakrishnan, V. Swamy, N. Mathews, P. P. Boix, S. G. Mhaisalkar, *Adv. Mater.* **2016**, *28*, 3653.

[60] Y. Tian, I. G. Scheblykin, *J. Phys. Chem. Lett.* **2015**, *6*, 3466.

[61] A. Latini, G. Gigli, A. Ciccioli, *Sustain. Energy Fuels* **2017**, *1*, 1351.

[62] E. J. Juarez-Perez, L. K. Ono, M. Maeda, Y. Jiang, Z. Hawash, Y. Qi, *J. Mater. Chem. A* **2018**, *6*, 9604.

SUPPORTING INFORMATIOM

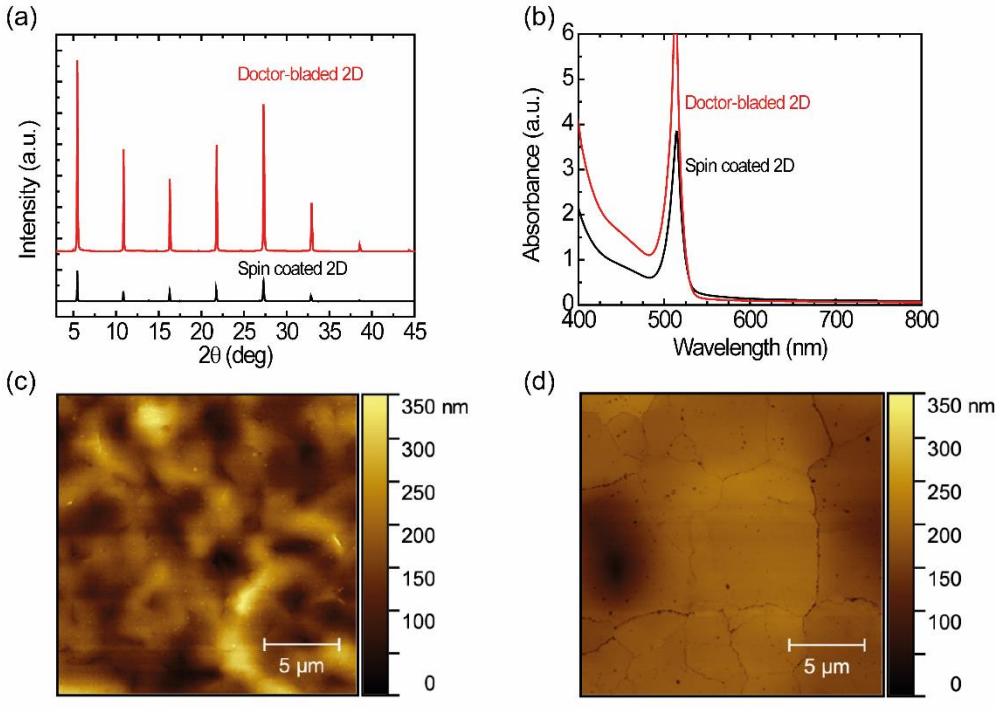

Fig. S1. Structural, optical and morphological characterization of spin coated and doctor-blade coated 2D PEA_2PbI_4 perovskite films on glass substrates. **(a)** X-ray diffraction patterns, **(b)** UV-vis absorbance spectra. AFM topological images of spin coated **(c)** and doctor-blade coated films (**d**).

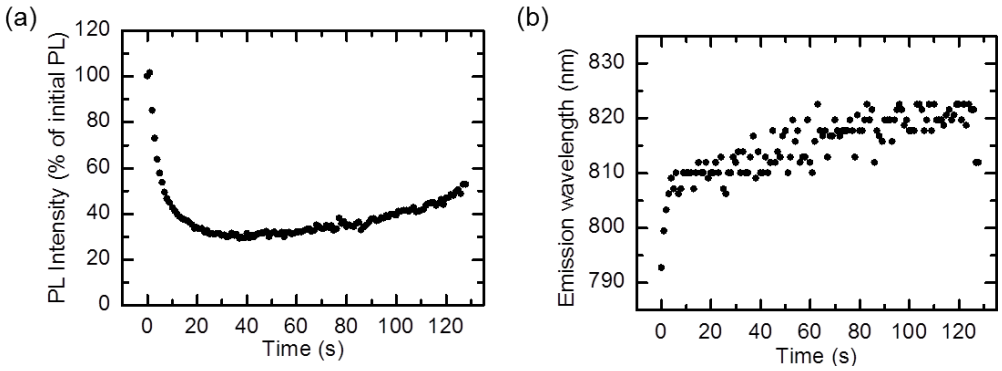

Fig. S2. Results of the Gaussian fitting to the 3D emission peak at different times during the conversion process. (a) The PL intensity normalized to the first occurrence of the 3D emission (100%) and (b) center of gravity of the fitted peak wavelength.

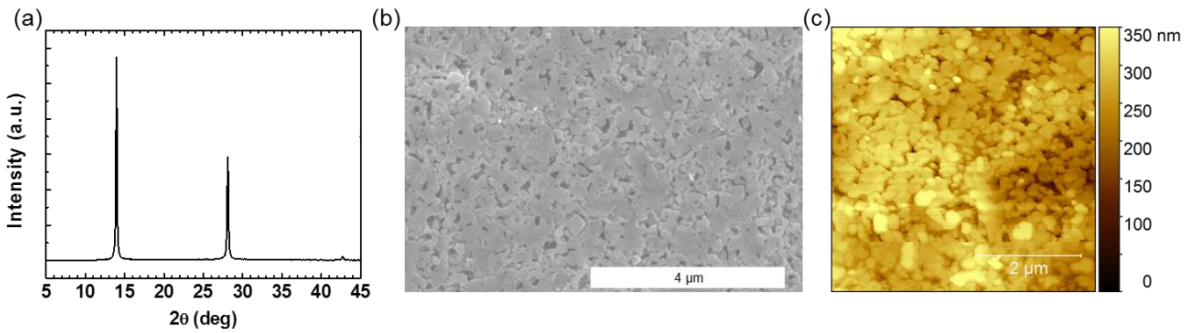

Fig. S3. Structural and morphological characterization of the converted 3D $FAPbI_3$ perovskite film based on spin coated 2D perovskite film. (a) X-ray diffraction pattern, (b) top-view SEM micrograph and (c) AFM image of the film.

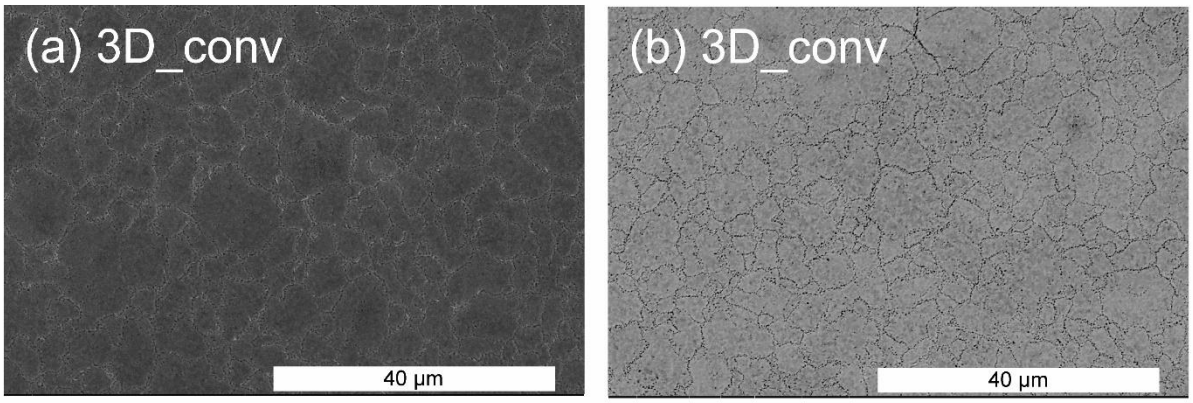

Fig. S4. SEM images showing a wider view of the surface topography and compositional properties of the converted perovskite film.

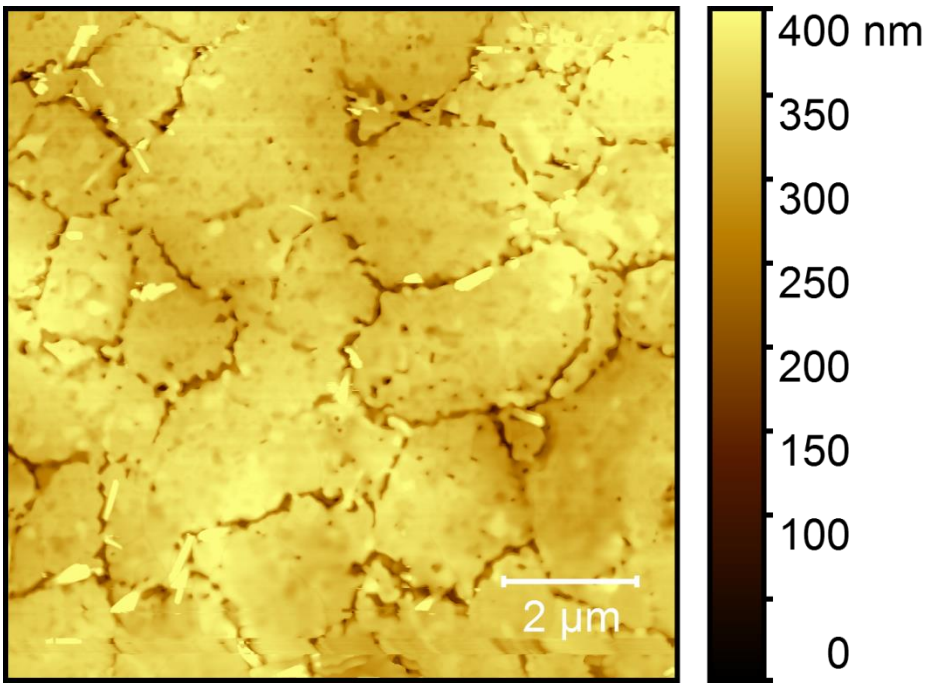

Fig. S5. AFM micrograph of the converted 3D $FAPbI_3$ perovskite film

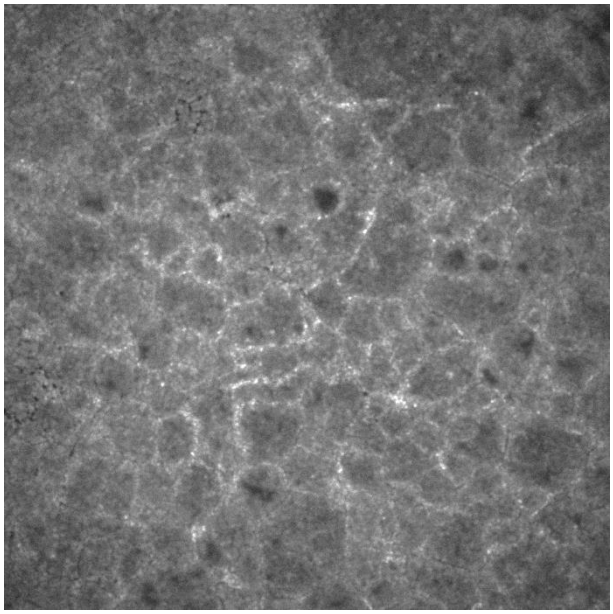

Fig. S6. Confocal laser scanning micrograph of the converted 3D $FAPbI_3$ perovskite film. Brighter colors indicate higher intensity of the PL. The image size is 100 x 100 μm^2.

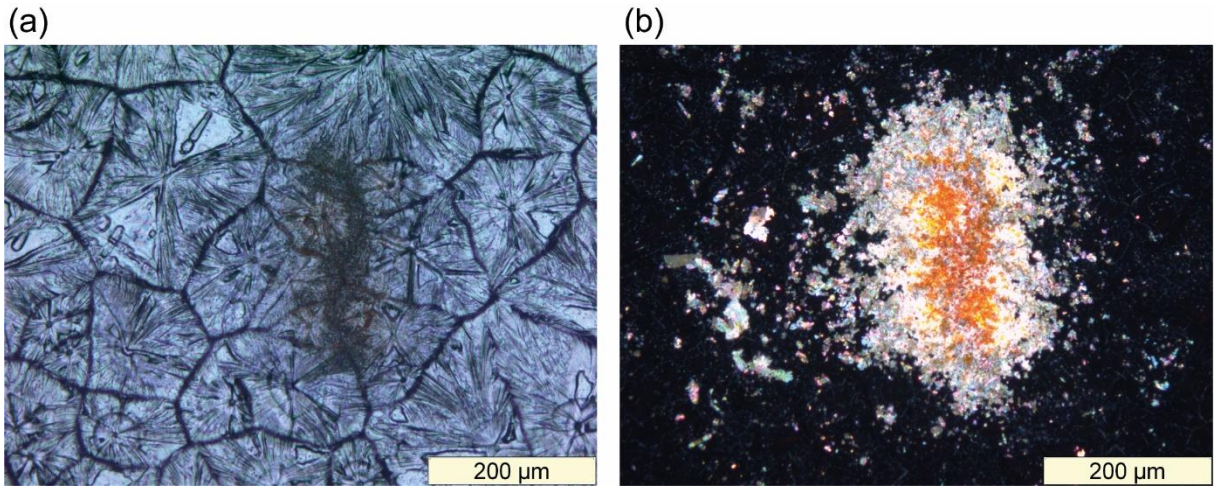

Fig. S7. Bright-field microscopy images showing the decomposition of the reference film under laser excitation (a) without and (b) under cross-polarization.

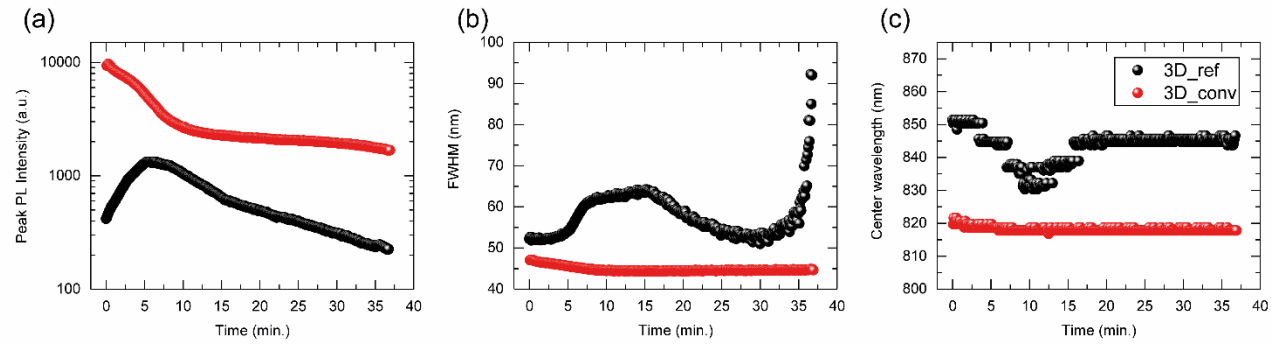

Fig. S8. PL parameters extracted from the data in Fig. 6a and 6b demonstrating the superior film quality of the converted film. **(a)** Peak intensity, **(b)** FWHM, and **(c)** center wavelength of the PL tracked over time. The sharp rise in the FWHM stems from the broad emission feature at high energy.